


Article

On-Line Detection of Demagnetization for Permanent Magnet Synchronous Motor via Flux Observer

Liqian Cao and Zhong Wu * 

School of Instrumentation and Optoelectronic Engineering, Beihang University, Beijing 100191, China; zy1917232clq@buaa.edu.cn

* Correspondence: wuzhong@buaa.edu.cn; Tel.: +86-10-8233-9703

Abstract: Demagnetization in permanent magnet synchronous motor (PMSM), caused by high temperature or inverse magnetic field, may increase loss and torque ripple, and even degrade the system stability in severe cases. On-line detection can identify the incipient demagnetization of permanent magnets (PMs), as well as providing reference for subsequent fault-tolerant control, so as to avoid further demagnetization. Therefore, an on-line demagnetization detection method is proposed in this paper by using flux observer. First, an observer is established in the three-phase stationary reference frame by taking the stator currents and the amplitudes of the fundamental and harmonic components of flux as state variables. Then, three demagnetization indexes are presented to evaluate the properties of PMs based on the observed flux information. The proposed method can directly track the amplitude of harmonic flux and evaluate the severity of the demagnetization more comprehensively. Simulation and experimental results demonstrate the effectiveness of the proposed method.

Keywords: permanent magnet synchronous motor; demagnetization; flux observer



Citation: Cao, L.; Wu, Z. On-Line Detection of Demagnetization for Permanent Magnet Synchronous Motor via Flux Observer. *Machines* **2022**, *10*, 354. <https://doi.org/10.3390/machines10050354>

Academic Editors: Hady H. Fayek and Christoph M. Hackl

Received: 13 April 2022

Accepted: 5 May 2022

Published: 9 May 2022

Publisher's Note: MDPI stays neutral with regard to jurisdictional claims in published maps and institutional affiliations.



Copyright: © 2022 by the authors. Licensee MDPI, Basel, Switzerland. This article is an open access article distributed under the terms and conditions of the Creative Commons Attribution (CC BY) license (<https://creativecommons.org/licenses/by/4.0/>).

1. Introduction

Permanent magnet synchronous motor (PMSM) is a kind of motor in which PMs are installed on the rotor to provide excitation. It does not need excitation current and it has no excitation loss. Therefore, PMSMs have the advantages of high electromagnetic torque, high efficiency, high power density and high-performance control. PMSMs are being used increasingly in a wide range of applications such as industrial servo drive, electric vehicle, aerospace and other fields [1,2].

However, high temperature can reduce magnetization of the rotor magnets [3] and over-current or short circuit can generate the inverse magnetic field, which is opposed to the remanent induction. All the cases will inevitably cause uniform demagnetization and local demagnetization [4,5]. Uniform demagnetization will only decrease the amplitudes of back electromotive forces (EMFs) and torque but not change their waveforms, as the symmetry of the equivalent physical structure of the motor is not affected. Local demagnetization not only decreases the amplitudes of back EMFs and torque, but also leads to waveform distortion of back EMFs and flux. Once demagnetization has occurred, the PMSMs tend to need a higher current to retain the same torque, which will increase the copper losses and the PMs temperature, resulting in further demagnetization [6]. Non-sinusoidal back EMFs will cause torque and speed pulsations which will degrade the system stability. For example, in the control moment gyroscopes, the torque ripple will seriously affect the high-precision and high stability control of the gimbal servo system. Therefore, it is very important to detect the magnetic properties of PMs regularly.

Many methods have been proposed to detect the demagnetization of PMs. The most direct method is to disassemble the motor and measure the flux distribution on the magnet surface with a Gauss meter. In addition, in order to avoid disassembling the motor, the

spectrum analysis of output data such as current [7–9] and back EMFs [10,11] have become the research trend. In the case of local demagnetization, there will be some fault harmonics in the output data, which are commonly used to detect demagnetization. However, some scholars have proved that the stator windings configuration will greatly affect the generation of fault harmonics such as fractional harmonics [12–15]. In [12–14], zero-sequence voltage component (ZSVC) was proposed to detect demagnetization, but the method required an available neutral point of the stator windings. In [16,17], a high-frequency signal injection technology is proposed, which uses the inverter to excite the motor with a pulsating field. It can be observed that the current peaks or the inductance pattern will produce a variation with the change of magnetic saturation due to demagnetization. However, the motor needs to be detected at standstill.

In order to observe the health status of the PMs online without the limitation of the configuration of the windings, on-line detection technologies based on flux observer have attracted considerable attentions. Various technologies, such as Kalman filter [18], extended Kalman filter [19], second-order generalized integral method [20], ANN-based flux observer [21] and adaptive flux observer [22], have been used to observe flux linkage of the motor. However, these papers only focused on the DC component or average value of flux while the waveform of the flux linkage was not considered. In [23,24], non-sinusoidal d-q axis flux linkages were observed by using the EKF-based observer, which took the d-q axis flux linkages as the state variables. However, only observing the change of waveform of the flux linkages cannot quantitatively distinguish and evaluate the demagnetization degree. Therefore, it is of great significance to obtain the harmonic flux and quantitatively detect and evaluate the demagnetization.

In this paper, a flux observer is proposed in the three-phase stationary reference frame, and the amplitude of each harmonic is taken as augmented state to observe the fundamental and harmonic components of the flux. Then, three demagnetization indexes are developed to comprehensively evaluate the degree of magnetic property degradation from two aspects of amplitude and waveform by using the observed flux information.

Compared with the current results in the field of demagnetization detection, the proposed method cannot only realize on-line detection of demagnetization, but also evaluate the demagnetization degree quantitatively considering both amplitude and waveform. Furthermore, this method is not limited to the stator winding configuration and can be applied to all types of PMSMs.

This paper is organized as follows: The influence of magnetic property degradation in PMSM is analyzed in Section 2. Section 3 presents the proposed demagnetization detection method via the flux observer. Simulation and experimental results are presented in Sections 4 and 5, respectively. Finally, the conclusion of the paper is given in Section 6.

2. Influence of Magnetic Property Degradation in PMSM

2.1. Influence on Back EMFs

In the three-phase stationary reference frame, the three-phase terminal voltage can be expressed as

$$\mathbf{u}_s = R\mathbf{i}_s + L\frac{d\mathbf{i}_s}{dt} + \mathbf{e} \quad (1)$$

where $\mathbf{u}_s = [u_a \ u_b \ u_c]^T$, $\mathbf{i}_s = [i_a \ i_b \ i_c]^T$ and $\mathbf{e} = [e_a \ e_b \ e_c]^T$ represent three-phase voltages, winding currents and back EMFs, respectively, R and L represent the phase resistance and inductance of stator winding, respectively.

The air gap magnetic field is produced by the combined action of winding current and PM field. The demagnetization phenomenon in PMs inevitably affects the amplitude and waveform of the air gap magnetic field. Usually, the flux linkage has half-wave symmetry

and even harmonics do not exist in the flux linkage, the non-sinusoidal flux λ_s can be expressed as

$$\lambda_s = \begin{bmatrix} \sum_{k=1}^{\infty} \lambda_{2k-1} \cos[(2k-1)\theta_e] \\ \sum_{k=1}^{\infty} \lambda_{2k-1} \cos[(2k-1)(\theta_e - \frac{2\pi}{3})] \\ \sum_{k=1}^{\infty} \lambda_{2k-1} \cos[(2k-1)(\theta_e + \frac{2\pi}{3})] \end{bmatrix} \quad (2)$$

where λ_{2k-1} represents the amplitude of harmonic component of flux and θ_e represents the electrical angle.

According to the law of the electromagnetic induction, the back EMFs can be calculated by

$$e = -\frac{d\lambda_s}{dt} = -\frac{d\lambda_s}{d\theta_e} \frac{d\theta_e}{dt} \quad (3)$$

Substitute Equation (2) into Equation (3), then the back EMFs can be rewritten as

$$e = \omega_e \begin{bmatrix} \sum_{k=1}^{\infty} \lambda_{2k-1} \sin[(2k-1)\theta_e] \\ \sum_{k=1}^{\infty} \lambda_{2k-1} \sin[(2k-1)(\theta_e - \frac{2\pi}{3})] \\ \sum_{k=1}^{\infty} \lambda_{2k-1} \sin[(2k-1)(\theta_e + \frac{2\pi}{3})] \end{bmatrix} \quad (4)$$

where ω_e represents the electrical rotor angular speed.

Define

$$\lambda_{amp} = [\lambda_1 \quad \lambda_3 \quad \lambda_5 \quad \dots]^T \quad (5)$$

$$\mathbf{B}(\theta_e) = \begin{bmatrix} \sin \theta_e & \sin 3\theta_e & \sin 5\theta_e & \dots \\ \sin(\theta_e - \frac{2\pi}{3}) & \sin(3(\theta_e - \frac{2\pi}{3})) & \sin(5(\theta_e - \frac{2\pi}{3})) & \dots \\ \sin(\theta_e + \frac{2\pi}{3}) & \sin(3(\theta_e + \frac{2\pi}{3})) & \sin(5(\theta_e + \frac{2\pi}{3})) & \dots \end{bmatrix} \quad (6)$$

Then, Equation (4) can be rewritten as

$$e = \omega_e \mathbf{B}(\theta_e) \lambda_{amp} \quad (7)$$

From Equation (4), it is known that the magnetic properties degradation of PM can reduce the amplitude and cause waveform distortion of back EMFs.

2.2. Influence on Electromagnetic Torque and Speed

Once demagnetized, the electromagnetic torque and rotor speed will also be affected. Therefore, the specific influences of demagnetization on torque and speed are analyzed below. According to magnetic co-energy, and ignoring the cogging torque, the electromagnetic torque can be expressed as

$$T_e = p \frac{d\lambda_s^T}{d\theta_e} i_s = \frac{e^T i_s}{\omega_m} \quad (8)$$

where p represents the number of pole pairs, ω_m represents the mechanical rotor angular speed and $\omega_e = p\omega_m$.

Usually, standard sinusoidal current is injected into the stator windings in traditional current control strategy, and the sinusoidal current can be expressed as

$$i_s = I_{amp} \mathbf{S}(\theta_e) \quad (9)$$

where $\mathbf{S}(\theta_e) = [\sin(\theta_e) \quad \sin(\theta_e - \frac{2\pi}{3}) \quad \sin(\theta_e + \frac{2\pi}{3})]^T$, and I_{amp} represents the current amplitude function.

We define $\boldsymbol{\mu} = e/\omega_m$ as back EMFs at unit speed, and substitute Equation (7) into it, then we obtain

$$\boldsymbol{\mu} = p\mathbf{B}(\boldsymbol{\theta}_e)\boldsymbol{\lambda}_{amp} \quad (10)$$

According to the definition of back EMFs at unit speed, Equation (8) can be rewritten as

$$T_e = \boldsymbol{\mu}^T \mathbf{i}_s \quad (11)$$

When the motor with a non-sinusoidal back EMFs waveform is controlled by sinusoidal current, the electromagnetic torque can be calculated from Equations (9)–(11) as

$$T_e = pI_{amp}\boldsymbol{\lambda}_{amp}^T \mathbf{B}^T(\boldsymbol{\theta}_e)\mathbf{S}(\boldsymbol{\theta}_e) \quad (12)$$

Substituting Equations (5) and (6) into Equation (12), it is easy to obtain the actual electromagnetic torque, which includes average torque and multiples of 6th harmonic torque.

$$T_e = T_c + \sum_{k=1}^{\infty} T_{6k} \cos(6k\theta_e) \quad (13)$$

where $T_c = \frac{3}{2}p\lambda_1 I_{amp}$ and $T_{6k} = \frac{3}{2}pI_{amp}(\lambda_{6k+1} - \lambda_{6k-1})$ represent the average torque and harmonic torque.

As shown in Equation (13), if flux distortion has occurred in the motor and we still control the system with the standard sinusoidal current, periodic ripples related to the rotor electrical angle in torque will occur and decrease the motor control performance.

In order to analyze the influence of demagnetization on rotor speed, the mechanical equation of PMSM is given as

$$T_e = J \frac{d\omega_m}{dt} + T_L + B\omega_m \quad (14)$$

From Equation (14), the torque harmonic can produce the speed harmonic of the same order [25]. The rotor speed can be decoupled into DC component and harmonic components, as shown in Equation (15).

$$\omega_m = \Omega_{m0} + \sum_{k=1}^{\infty} \Omega_{mk} \cos(6k\theta_e) \quad (15)$$

where Ω_{m0} and Ω_{mk} represent the DC component and harmonic components of speed, respectively.

As shown in Equation (15), there are periodic ripples related to rotor electrical angle in torque which are not expected to appear in high-performance control system. Therefore, it is necessary to detect the magnetic properties of PMs online.

3. Demagnetization Detection Method

In order to detect the health of PMs, a flux observer is established to obtain the amplitude of fundamental component and harmonic components of flux at first. Then, three demagnetization indexes are established to evaluate the demagnetization degree by using the observed flux information.

3.1. Flux Observer

In order to design the flux observer, Equation (1) can be rewritten in the following form by substituting Equation (7) as

$$L\dot{\mathbf{i}}_s = -R\mathbf{i}_s - \omega_e \mathbf{B}(\boldsymbol{\theta}_e)\boldsymbol{\lambda}_{amp} + \mathbf{u}_s \quad (16)$$

According to Equation (16), the observer is designed as follows.

$$L\dot{\hat{\mathbf{i}}}_s = -R\hat{\mathbf{i}}_s - \omega_e \mathbf{B}(\theta_e) \hat{\lambda}_{amp} + \mathbf{u}_s + \rho(\mathbf{i}_s - \hat{\mathbf{i}}_s) \quad (17)$$

$$\dot{\hat{\lambda}}_{amp} = -\alpha \omega_e \mathbf{B}^T(\theta_e)(\mathbf{i}_s - \hat{\mathbf{i}}_s) \quad (18)$$

where $\hat{\mathbf{i}}_s$ and $\hat{\lambda}_{amp}$ represent the estimates of current and flux, respectively. The gain coefficients α and ρ are positive constants.

Let $\tilde{\mathbf{i}}_s = \mathbf{i}_s - \hat{\mathbf{i}}_s$ and $\tilde{\lambda}_{amp} = \lambda_{amp} - \hat{\lambda}_{amp}$ represent the current error and flux error, respectively, then the error dynamic equations of the observer can be derived from Equations (16)–(18) as

$$L\dot{\tilde{\mathbf{i}}}_s = -(R + \rho)\tilde{\mathbf{i}}_s - \omega_e \mathbf{B}(\theta_e) \tilde{\lambda}_{amp} \quad (19)$$

$$\dot{\tilde{\lambda}}_{amp} = \alpha \omega_e \mathbf{B}^T(\theta_e) \tilde{\mathbf{i}}_s \quad (20)$$

We choose Lyapunov candidate function for the error system as

$$V = \frac{1}{2} \tilde{\mathbf{i}}_s^T L \tilde{\mathbf{i}}_s + \frac{1}{2} \tilde{\lambda}_{amp}^T \tilde{\lambda}_{amp} > 0 \quad (21)$$

Taking the time derivative of Equation (21) along Equations (19) and (20), we obtain

$$\begin{aligned} \dot{V} &= \tilde{\mathbf{i}}_s^T L \dot{\tilde{\mathbf{i}}}_s + \tilde{\lambda}_{amp}^T \dot{\tilde{\lambda}}_{amp} \\ &= -\alpha(R + \rho) \tilde{\mathbf{i}}_s^T \tilde{\mathbf{i}}_s - \alpha \omega_e \tilde{\mathbf{i}}_s^T \mathbf{B}(\theta_e) \tilde{\lambda}_{amp} + \tilde{\lambda}_{amp}^T \tilde{\lambda}_{amp} \\ &= -\alpha(R + \rho) \tilde{\mathbf{i}}_s^T \tilde{\mathbf{i}}_s \leq 0 \end{aligned} \quad (22)$$

Since $\dot{V} \leq 0$, it is clear that $V(t) \leq V(0)$. According to Equation (21), it is known that both $\tilde{\mathbf{i}}_s$ and $\tilde{\lambda}_{amp}$ are bounded. Then, the bounded $\dot{\tilde{\mathbf{i}}}_s$ can be obtained from Equation (19). Taking the derivative of Equation (22) gives $\ddot{V} = -2\alpha(R + \rho) \tilde{\mathbf{i}}_s^T \dot{\tilde{\mathbf{i}}}_s$. Thus, the bounded $\tilde{\mathbf{i}}_s$ and $\dot{\tilde{\mathbf{i}}}_s$ can guarantee that \ddot{V} is also bounded. According to Barbalat Lemma, it can be known that $\dot{V} \rightarrow 0$ when $t \rightarrow \infty$. Correspondingly, $\tilde{\mathbf{i}}_s$ will converge to 0 when $t \rightarrow \infty$ according to Equation (22).

Under the steady-state assumption of the flux observer, the following equation can be approximately deduced from Equation (19) as

$$\tilde{\mathbf{i}}_s = -(R + \rho)^{-1} \omega_e \mathbf{B}(\theta_e) \tilde{\lambda}_{amp} \quad (23)$$

Substituting Equation (23) into Equation (20) gives

$$\dot{\tilde{\lambda}}_{amp} = -\alpha \omega_e^2 (R + \rho)^{-1} \mathbf{B}^T(\theta_e) \mathbf{B}(\theta_e) \tilde{\lambda}_{amp} \quad (24)$$

According to the definition of the matrix $\mathbf{B}(\theta_e)$, it is easy to verify that $\mathbf{B}^T(\theta_e) \mathbf{B}(\theta_e)$ is persistently exciting. According to Theorem 1 in [26], it can be known that $\tilde{\lambda}_{amp}$ also can converge to 0 when $t \rightarrow \infty$.

In addition, the gain coefficients ρ and α can be used to regulate the convergence rate of the observer. Form Equation (24), it easy to know that a bigger α and a smaller ρ will result in a faster convergence of $\tilde{\lambda}_{amp}$.

3.2. Demagnetization Index

In order to comprehensively evaluate the demagnetization degree, three demagnetization indexes are presented to evaluate the severity of the demagnetization. The fundamental

flux accounts for the largest proportion, thus, the rate of the fundamental flux variation is generally defined as the demagnetization index.

Index I: Demagnetization rate η_{dem}

$$\eta_{dem} = \frac{|\lambda_{1-dem} - \lambda_{1-health}|}{\lambda_{1-health}} \times 100\% \quad (25)$$

where λ_{1-dem} and $\lambda_{1-health}$ represent the value of fundamental component of flux in demagnetization motor and the value of fundamental component of flux in healthy motor, respectively.

Considering that local demagnetization leads to flux distortion, total harmonic distortion (THD) is proposed to evaluate the degree of magnetic property degradation.

Index II: Total harmonic distortion THD

$$THD = \frac{\sqrt{\sum_{k=2}^n \lambda_k^2}}{\lambda_1} \times 100\% \quad (26)$$

where λ_k and λ_1 represent the value of the k th harmonic of flux and the value of fundamental component of flux, respectively.

In addition, there will be obvious variation in a certain harmonic of flux with the deepening of demagnetization. In [27], the 5th harmonic with obvious variation is used to evaluate the severity of the demagnetization. Therefore, the change rate of flux harmonic with largest variation is selected as the Index III.

Index III: Change rate of variation maximum harmonic δ

$$\delta = \max\left(\frac{|\lambda_k - \lambda_{k-health}|}{\lambda_{k-health}} \times 100\%\right) \quad (27)$$

where λ_k and $\lambda_{k-health}$ represent the k th harmonic amplitude of the flux linkage at the current time and healthy time of the motor.

To sum up, the three demagnetization indexes can achieve a more comprehensive demagnetization evaluation from amplitude and waveform by using the observed flux information.

4. Simulation Results

In the simulation, a surface-mounted permanent magnet synchronous motor (SPMSM) with two pole pairs is taken as the test motor. The phase resistance is 1.2Ω , the phase inductance is 2 mH , the damping coefficient is $4.8 \times 10^{-4} \text{ Nm}/(\text{rad}\cdot\text{s}^{-1})$, and the inertia of motor is $5.8 \times 10^{-3} \text{ Kg}\cdot\text{m}^2$. The test motor operates at 0.5 rad/s .

Different demagnetization cases are simulated by changing the amplitude of fundamental flux and 5th, 7th and 11th harmonic flux. The amplitude of each harmonic is reduced to the same extent to simulate uniform demagnetization and different variations of different harmonics are used to simulate local demagnetization.

According to the above description, different demagnetization schemes are set, and the detailed parameters are as follows:

- (1) Healthy motor: $\lambda_1 = 0.31 \text{ Wb}$, $\lambda_5 = 6.75 \times 10^{-3} \text{ Wb}$, $\lambda_7 = 5.34 \times 10^{-3} \text{ Wb}$, $\lambda_{11} = 3.18 \times 10^{-3} \text{ Wb}$;
- (2) Uniform demagnetization: uniform reduction of 25% and 50% of each harmonic of flux in healthy motor;
- (3) Twenty-five-percent local demagnetization motor: $\lambda_1 = 0.23 \text{ Wb}$, $\lambda_5 = 9.25 \times 10^{-3} \text{ Wb}$, $\lambda_7 = 5.04 \times 10^{-3} \text{ Wb}$, $\lambda_{11} = 3.45 \times 10^{-3} \text{ Wb}$;
- (4) Fifty-percent local demagnetization motor: $\lambda_1 = 0.16 \text{ Wb}$, $\lambda_5 = 1.13 \times 10^{-2} \text{ Wb}$, $\lambda_7 = 4.78 \times 10^{-3} \text{ Wb}$, $\lambda_{11} = 3.56 \times 10^{-3} \text{ Wb}$.

4.1. Influence Analysis of Magnetic Property Degradation

The influences of uniform demagnetization on back EMFs, torque and speed are shown in Figures 1–3. From Figure 1, it can be seen that the waveform of the back EMFs remains unchanged, while its amplitude is decreased with the degree of demagnetization becoming deeper. From Figures 2 and 3, it can be seen that uniform demagnetization does not increase the torque and speed ripple.

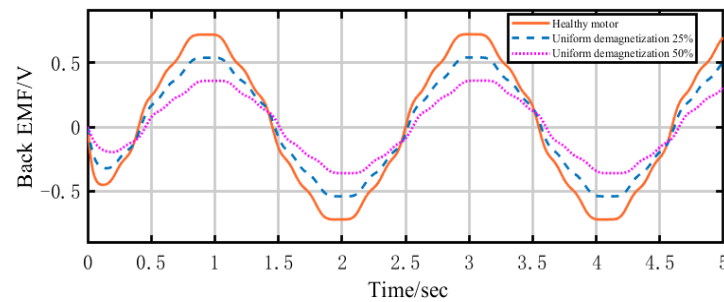


Figure 1. Influence of uniform demagnetization on back EMFs.

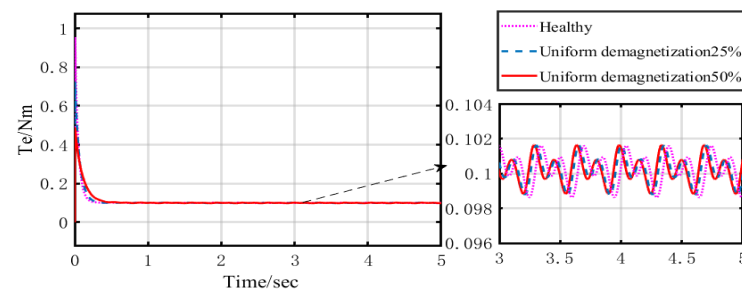


Figure 2. Influence of uniform demagnetization on torque.

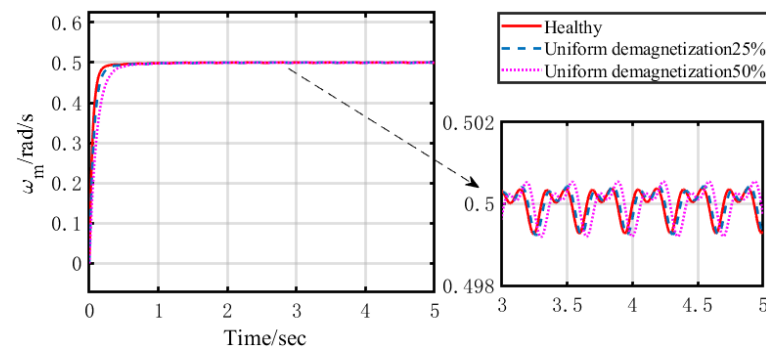


Figure 3. Influence of uniform demagnetization on speed.

The influences of local demagnetization on back EMFs, torque and speed are shown in Figures 4–6. From Figure 4, it can be seen that the degree of waveform distortion of the back EMFs is deeper, and the amplitude is decreased with the degree of demagnetization becoming deeper. From Figures 5 and 6, it can be seen that the torque and speed ripple increase gradually with the deepening of demagnetization.

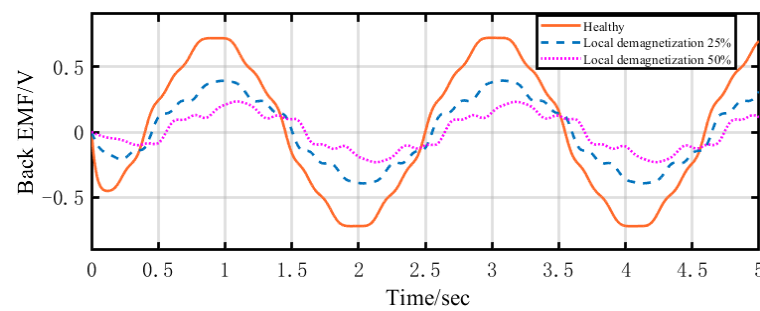


Figure 4. Influence of local demagnetization on back EMFs.

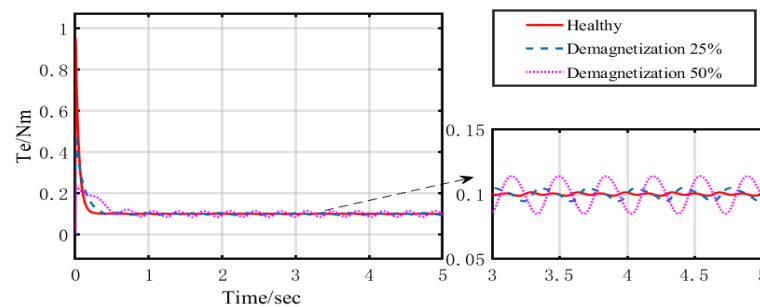


Figure 5. Influence of local demagnetization on torque.

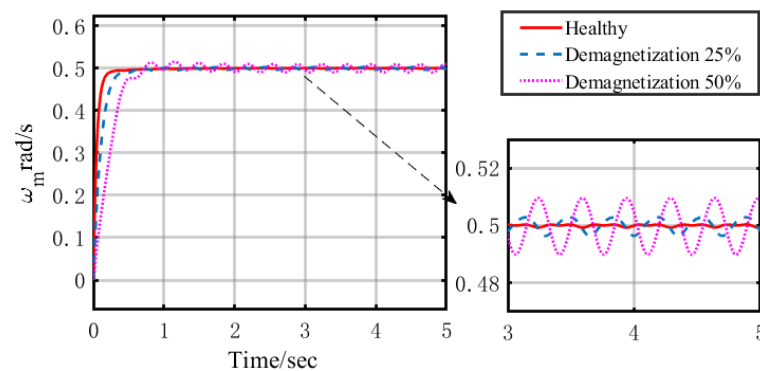


Figure 6. Influence of local demagnetization on speed.

4.2. Proposed Detection Method

The effectiveness and advantages on demagnetization detection and severity assessment ought to be verified. An observer proposed in [22] is compared under the same demagnetization conditions as Section 4.1. The observer chooses the stator currents and d-q axis flux linkage as state variables. In this paper, the stator currents and amplitudes of harmonic flux are selected as state variables.

Under the same uniform demagnetization conditions, the waveforms of d-q axis flux linkage obtained by the compared flux observer are shown in the Figure 7, and the amplitudes of harmonics flux obtained by the proposed flux observer are shown in the Figure 8. With the deepening of demagnetization, both observers can clearly observe that the amplitudes of flux decrease and the waveforms remain unchanged. However, the proposed observer can observe the variation of each harmonic, which cannot be observed by the compared observer.

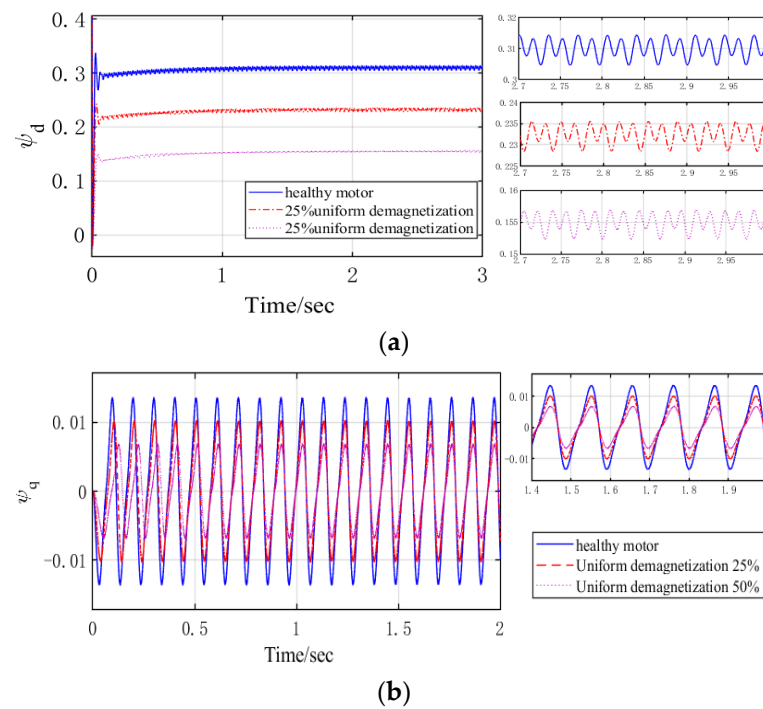


Figure 7. Flux waveform observation under different degrees of uniform demagnetization (compared flux observer): (a) d-axis flux linkage; (b) q-axis flux linkage.

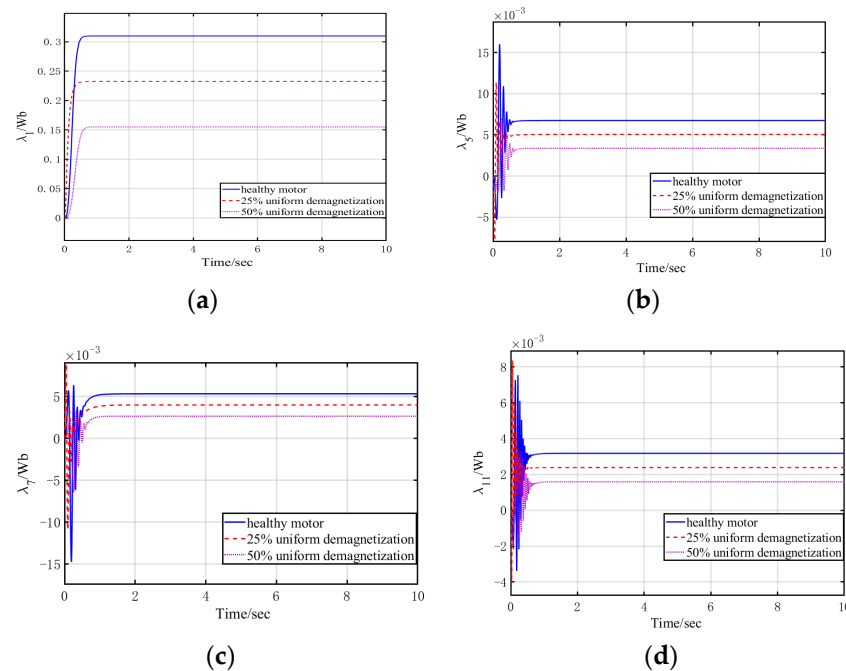


Figure 8. Flux observation under different degrees of uniform demagnetization (proposed observer): (a) Fundamental component observation; (b) Fifth harmonic observation; (c) Seventh harmonic observation; (d) Eleventh harmonic observation.

Under the same local demagnetization conditions, the waveforms of d-q axis flux linkage obtained by the compared flux observer are as shown in Figure 9, and the amplitudes of harmonics flux obtained by the proposed flux observer are shown in Figure 10. From Figure 9a, it can be seen that the amplitude of d-axis flux linkage decreases obviously with the deepening of demagnetization. However, the demagnetization cannot be analyzed quantitatively. There is no significant change in the waveform of q-axis flux linkage, es-

pecially in low demagnetization state. In contrast, the variation of each harmonic is clear in Figure 10. Therefore, the proposed method can quantitatively detect and evaluate the demagnetization of permanent magnet synchronous motors on-line by using the estimated information from the flux observer.

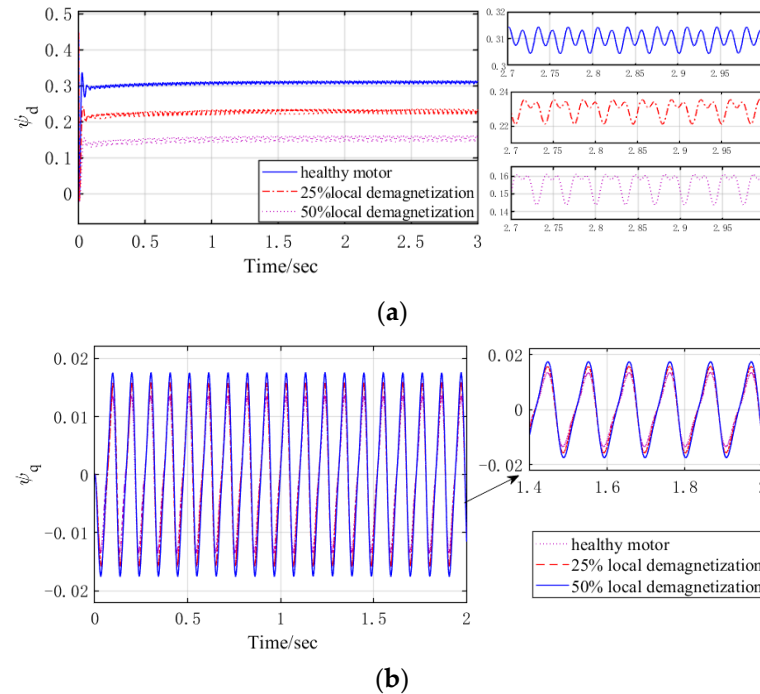


Figure 9. Flux waveform observation under different degrees of local demagnetization (conventional flux observer): (a) d-axis flux linkage; (b) q-axis flux linkage.

Then, the data of 8–10 s are selected at steady state, and the average value is taken as the observation results which are recorded in Table 1. As shown in Table 1, the observed amplitude of each harmonic is consistent with the set value. Comparing case1, case2 and case3, it can be observed that each harmonic flux has the same change rate in the same case. According to index I, $\eta_{dem-2} = 25\%$ and $\eta_{dem-3} = 50\%$, which are consistent with the real degree. According to index II, $THD_1 = 2.98\%$, $THD_2 = 2.99\%$, $THD_3 = 2.99\%$, $THD_4 = 5.8\%$ and $THD_5 = 8.3\%$. According to the calculated values, it can be seen that uniform demagnetization does not affect its distortion degree, and an increasing degree of local demagnetization results in an increasing of distortion degree. The variations of case 4 and case 5 are different, and the variation of 5th harmonic of flux is the largest. According to index III, $\delta_4 = 0.37$ and $\delta_5 = 0.66$, from which it can be inferred that case 5 has a higher degree of demagnetization.

Table 1. Observation results of amplitude of flux linkage.

Parameter	Case 1	Case 2	Case 3	Case 4	Case 5
λ_1 (Wb)	0.31	0.23	0.16	0.23	0.16
λ_5 (Wb)	6.75×10^{-3}	5.06×10^{-3}	3.38×10^{-3}	9.25×10^{-3}	1.12×10^{-2}
λ_7 (Wb)	5.35×10^{-3}	4.01×10^{-3}	2.68×10^{-3}	5.04×10^{-3}	4.78×10^{-3}
λ_{11} (Wb)	3.17×10^{-3}	2.38×10^{-3}	1.59×10^{-3}	3.44×10^{-3}	3.54×10^{-3}

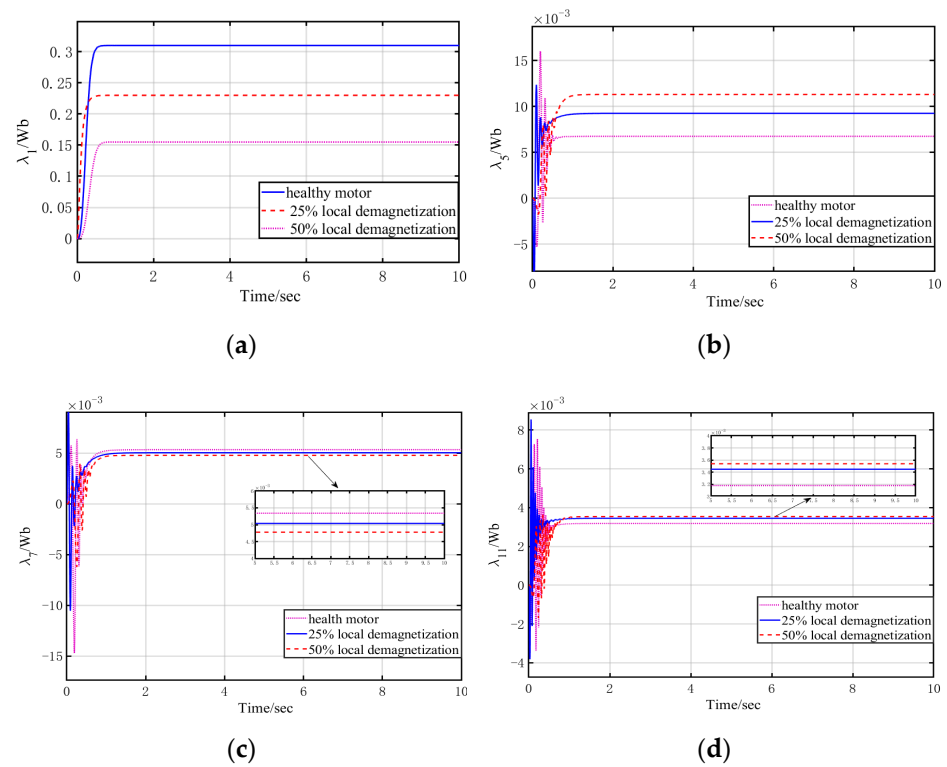


Figure 10. Flux observation under different degrees of local demagnetization. (a) Fundamental component observation; (b) Fifth harmonic observation; (c) Seventh harmonic observation; (d) Eleventh harmonic observation.

5. Experimental Results

The platform for the experiment is shown in Figure 11 and the given parameters of the PMSM are listed in Table 2. The physical experiment platform is composed of DSP driver board, permanent magnet synchronous motor, resolver and power supply. The modulation method is SPWM, the switching frequency is 15 kHz, and the sampling frequency is 1 kHz. The motor operates at 90 rad/s.

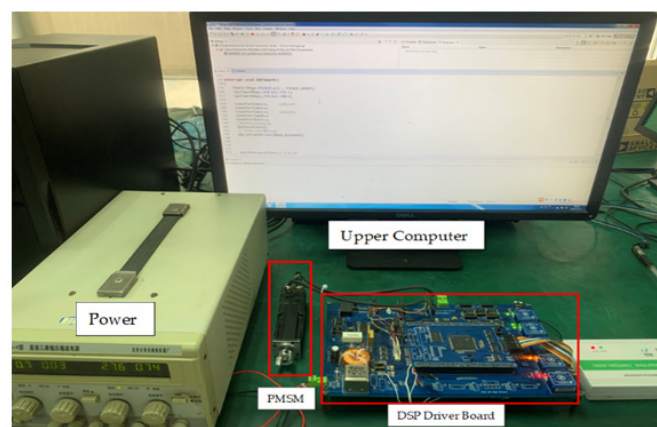


Figure 11. Experiment platform.

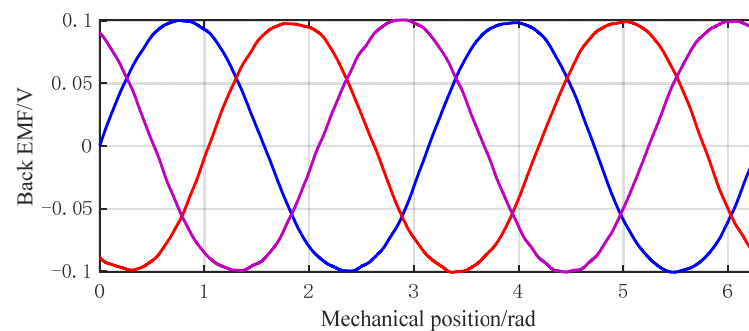
The motor in the laboratory had not been used for a long time and is still a healthy motor, so it can be considered that the flux mainly contains fundamental component, and the harmonic components are very little. According to the motor parameters in Table 2, the fundamental component of flux can be calculated. Given $k_e = 0.09 \text{ V/rad}\cdot\text{s}^{-1}$ and according to the equation $e = -\omega_e \mathbf{B}(\theta_e) \lambda_{amp} = k_e \omega_m$, the fundamental harmonic of flux $\lambda_1 = 0.045 \text{ Wb}$.

Table 2. Motor parameters and resolver parameters.

PMSM Parameters		Resolver Parameters	
Pole pairs	2	Pole pairs	1
Phase resistance	3 Ω	Input voltage	5 V \pm 0.2 (AC)
Phase inductance	1 mH	Input frequency	10 kHz
Rated speed	3000 r/min	Output voltage	>2 V
Back EMF coefficient	0.09 V/rad·s ⁻¹	Transformer ratio	0.5 \pm 5°
Sliding friction torque	0.06 Nm	Zero deviation	$\leq 10'$

In order to obtain the observation of flux linkage information, three-phase current, three-phase voltage, angular speed and angular position information are needed. The input voltage of the inverter is equivalent to three-phase voltage, and the rest of the information can be obtained by sampling and using a 16-bit AD8568 conversion chip.

Since the test motor is healthy, the off-line back EMFs of the test PMSM are obtained in advance, as shown in Figure 12.

**Figure 12.** Waveforms of back EMFs of PMSM at unit speed.

The results observed by the flux observer are presented in Figure 13. The average value of each harmonic in Figure 13 is calculated by using the data from 4 s to 5 s at steady state and then listed in Table 3.

Table 3. Comparison between actual and observed values.

Parameter	Observed Value
λ_1 (Wb)	0.0449
λ_3 (Wb)	3.43×10^{-5}
λ_5 (Wb)	1.89×10^{-9}
λ_7 (Wb)	1.19×10^{-9}

It is known that the observed fundamental component of flux is close to the actual value. The 3rd harmonic is very little, while the 5th and 7th harmonics are almost 0. According to the observed results, Index I can be calculated as $\eta_{dem} = 99.8\%$ which means that the motor is a healthy one. If the motor is replaced with a demagnetized motor, the proposed detection method is still valid. However, the relevant experiments were not carried out due to the limited experimental conditions.

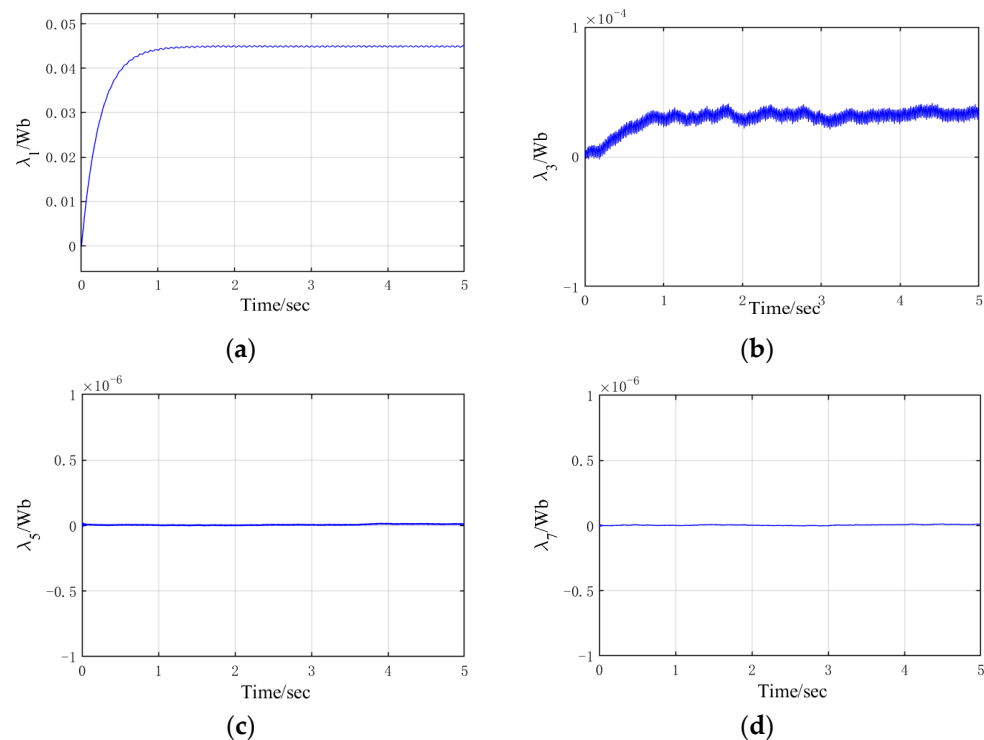


Figure 13. Observation results among real motors. (a) First harmonic observation; (b) Third harmonic observation; (c) Fifth harmonic observation; (d) Seventh harmonic observation.

6. Conclusions

In order to realize the on-line detection of magnetic properties of PMs and evaluate the demagnetization degree, an on-line demagnetization detection method is proposed in this paper via flux observer. Firstly, this paper analyzes the influence of magnetic property degradation on the performance of PMSM from local demagnetization and uniform demagnetization. Then, a flux observer is built in a three-phase stationary reference frame. This flux observer takes the flux harmonic amplitudes as the augmented states, and it can estimate the fundamental component and harmonic components of the flux quickly and accurately. Therefore, the flux observation proposed in this paper can obtain more comprehensive flux information and evaluate the demagnetization degree quantitatively based on proposed demagnetization index. Simulation and experimental results verify the accuracy of the observer. Although only SPMSM is used in the simulation and experiment, the proposed method can also be applied to motors of other types.

Author Contributions: Conceptualization, Z.W.; methodology, L.C.; validation, L.C.; writing—original draft preparation, L.C. and Z.W. All authors have read and agreed to the published version of the manuscript.

Funding: This research received no external funding.

Data Availability Statement: Not applicable.

Conflicts of Interest: The authors declare no conflict of interest.

References

1. Ehsani, M.; Rahman, K.M.; Toliyat, H.A. Propulsion system design of electric and hybrid vehicles. *IEEE Trans. Ind. Electron.* **1997**, *44*, 19–27. [[CrossRef](#)]
2. Lu, X.; Iyer, K.L.V.; Mukherjee, K.; Ramkumar, K.; Kar, N.C. Investigation of permanent-magnet motor drives incorporating damper bars for electrified vehicles. *IEEE Trans. Ind. Electron.* **2015**, *62*, 3234–3244. [[CrossRef](#)]
3. Tianze, M.; Pinjia, Z. A review of thermal monitoring techniques for radial permanent magnet machines. *Machines* **2021**, *10*, 18.

4. Reigosa, D.; Fernández, D.; Martínez, M.; Park, Y.; Lee, S.B.; Briz, F. Permanent magnet synchronous machine non-uniform demagnetization detection using zero-sequence magnetic field density. *IEEE Trans. Ind. Appl.* **2019**, *55*, 3823–3833. [[CrossRef](#)]
5. Mengoni, M.; Vancini, L.; Tani, A.; Gritli, Y.; Zarri, L.; Rossi, C. On-line detection of magnet demagnetization in asymmetrical six-phase surface-mounted permanent magnet synchronous motor drives. In Proceedings of the 2019 IEEE 12th International Symposium on Diagnostics for Electrical Machines, Power Electronics and Drives (SDEMPED), Toulouse, France, 27–30 August 2019; pp. 188–194.
6. Kim, K.C.; Lim, S.B.; Koo, D.H.; Ju, L. The shape design of permanent magnet for permanent magnet synchronous motor considering partial demagnetization. *IEEE Trans. Magn.* **2006**, *42*, 3485–3487. [[CrossRef](#)]
7. Ruiz, J.; Rosero, J.A.; Espinosa, A.G.; Romeral, L. Detection of demagnetization faults in permanent-magnet synchronous motors under nonstationary conditions. *IEEE Trans. Magn.* **2009**, *45*, 2961–2969. [[CrossRef](#)]
8. Le Roux, W.; Harley, R.G.; Habetler, T.G. Detecting rotor faults in low power permanent magnet synchronous machines. *IEEE Trans. Power Electron.* **2007**, *22*, 322–328. [[CrossRef](#)]
9. Krichen, M.; Elbouchikhi, E.; Naourez, B.; Chaieb, M.; Neji, R. Motor current signature analysis-based permanent magnet synchronous motor demagnetization characterization and detection. *Machines* **2020**, *8*, 35. [[CrossRef](#)]
10. Gritli, Y.; Rossi, C.; Casadei, D.; Zarri, L.; Filippetti, F. Demagnetization diagnosis for permanent magnet synchronous motors based on advanced wavelet analysis. In Proceedings of the 2012 International Conference on Electrical Machines, Marseille, France, 2–5 September 2012; pp. 2397–2403.
11. Candelozuluaga, C.; Riba, J.R.; Thangamuthu, D.V.; Garcia, A. Detection of partial demagnetization faults in five-phase permanent magnet assisted synchronous reluctance machines. *Energies* **2020**, *13*, 3496. [[CrossRef](#)]
12. Urresty, J.C.; Ruiz, J.R.; Romeral, L. A back-emf based method to detect magnet failures in PMSMs. *IEEE Trans. Magn.* **2012**, *49*, 591–598. [[CrossRef](#)]
13. Urresty, J.C.; Riba, J.R.; Delgado, M.; Romeral, L. Detection of demagnetization faults in surface-mounted permanent magnet synchronous motors by means of the zero-sequence voltage component. *IEEE Trans. Energy Convers.* **2012**, *27*, 42–51. [[CrossRef](#)]
14. Urresty, J.C.; Riba, J.R.; Romeral, L. Influence of the stator windings configuration in the currents and zero-sequence voltage harmonics in permanent magnet synchronous motors with demagnetization faults. *IEEE Trans. Magn.* **2013**, *49*, 4885–4893. [[CrossRef](#)]
15. Casadei, D.; Filippetti, F.; Rossi, C.; Stefani, A. Magnets faults characterization for permanent magnet synchronous motors. In Proceedings of the IEEE International Symposium on Diagnostics for Electric Machines, Power Electronics and Drives, Cargese, France, 31 August–3 September 2009; pp. 1–6.
16. Hong, J.; Hyun, D.; Lee, S.B.; Yoo, J.Y.; Lee, K.W. Automated monitoring of magnet quality for permanent-magnet synchronous motors at standstill. *IEEE Trans. Ind. Appl.* **2010**, *46*, 1397–1405. [[CrossRef](#)]
17. Hong, J. Detection and classification of rotor demagnetization and eccentricity faults for PM synchronous motors. *IEEE Trans. Ind. Appl.* **2012**, *48*, 923–932. [[CrossRef](#)]
18. Xiao, X.; Zhang, M.; Li, Y.; Li, M. On-line estimation of permanent magnet flux linkage ripple for PMSM based on a Kalman filter. In Proceedings of the 32nd Annual Conference on IEEE Industrial Electronics, Paris, France, 6–10 November 2006; pp. 1171–1175.
19. Min, Y.; Huang, W.; Yang, J.; Zhao, Y. On-line estimation of permanent-magnet flux and temperature rise in stator winding for PMSM. In Proceedings of the 22nd International Conference on Electrical Machines and Systems (ICEMS), Harbin, China, 11–14 August 2019; pp. 1–5.
20. Xu, W.; Jiang, Y.; Mu, C.; Blaabjerg, F. Improved nonlinear flux observer-based second-order SOIFO for PMSM sensorless control. *IEEE Trans. Power Electron.* **2019**, *34*, 565–579. [[CrossRef](#)]
21. Kashif, S.A.R.; Saqib, M.A. ANN-based flux observer for the sensor-less control of a permanent magnet synchronous motor. In Proceedings of the 20th Australasian Universities Power Engineering Conference, Christchurch, New Zealand, 5–8 December 2010; pp. 1–6.
22. Uddin, M.N.; Zou, H.; Azevedo, F. Online loss minimization based adaptive flux observer for direct torque and flux control of PMSM drive. *IEEE Trans. Ind. Appl.* **2016**, *52*, 425–431. [[CrossRef](#)]
23. Xiao, X.; Chen, C.; Zhang, M. Magnet demagnetization observation or permanent magnet synchronous motor. In Proceedings of the International Conference on Electrical Machines and Systems, Wuhan, China, 17–20 October 2008; pp. 3216–3219.
24. Xiao, X.; Chen, C. Reduction of torque ripple due to demagnetization in PMSM using current compensation. *IEEE Trans. Appl. Supercond.* **2010**, *20*, 1068–1071. [[CrossRef](#)]
25. Feng, G.; Lai, C.; Mukherjee, K.; Kar, N.C. Online PMSM magnet flux-linkage estimation for rotor magnet condition monitoring using measured speed harmonics. *IEEE Trans. Ind. Appl.* **2017**, *53*, 2786–2794. [[CrossRef](#)]
26. Anderson, B. Exponential stability of linear equations arising in adaptive identification. *IEEE Trans. Autom. Control* **1977**, *22*, 83–88. [[CrossRef](#)]
27. Ullah, Z.; Lee, S.T.; Siddiqi, M.R.; Hur, J. Online diagnosis and severity estimation of partial and uniform irreversible demagnetization fault in interior permanent magnet synchronous motor. In Proceedings of the 2019 IEEE Energy Conversion Congress and Exposition (ECCE), Baltimore, MD, USA, 29 September–3 October 2019; pp. 1682–1686.